Journal of Materials Chemistry A

Conjugated Polymers with Controllable Interfacial Order and Energetics enable Tunable Heterojunctions in Organic and Colloidal Quantum Dot Photovoltaics

Journal:	*Journal of Materials Chemistry A*
Manuscript ID	TA-ART-11-2021-009544.R1
Article Type:	Paper
Date Submitted by the Author:	14-Dec-2021
Complete List of Authors:	Zhong, Yufei; NingboTech University, School of Materials Science and Engineering (MSE); King Abdullah University of Science and Technology, Division of Physical Sciences and Engineering Kirmani, Ahmad; King Abdullah University of Science and Technology (KAUST), Division of Physical Sciences and Engineering Lan, Xinzheng; Huazhong University of Science and Technology, School of Optical and Electronic Information and Wuhan National Laboratory for Optoelectronics (WNLO) Carpenter, Joshua; North Carolina State University Chew, Annabel; Stanford University Awartani, Omar ; North Carolina State University, Physics Yu, Liyang; Sichuan University; King Abdullah University of Science and Technology, Division of Physical Sciences and Engineering Niazi, Muhammad; King Abdullah University of Science and Technology, Division of Physical Sciences and Engineering Voznyy, Oleksandr; University of Toronto Scarborough, Physical and Environmental Sciences Hu, Hanlin; Shenzhen Polytechnic, Hoffman Institute of Advanced Materials; King Abdullah University of Science and Technology, Division of Physical Sciences and Engineering Ngongang Ndjawa, Guy; King Abdullah University of Science and Technology, Division of Physical Sciences and Engineering Tietze, Max ; University of Leuven, Centre for Membrane Separations, Adsorption, Catalysis and Spectroscopy for Sustainable Solutions (cMACS); King Abdullah University of Science and Technology, Division of Physical Sciences and Engineering Salleo, Alberto; Stanford University, Department of Materials Science and Engineering Ade, Harald; North Carolina State University, Physics Sargent, Edward; Canada Research Chair in Nanotechnology, Edward S. Rogers Sr. Department of Electrical Computer Engineering Amassian, Aram; North Carolina State University, Materials Science and Engineering; King Abdullah University of Science and Technology, Division of Physical Sciences and Engineering

Conjugated Polymers with Controllable Interfacial Order and Energetics enable Tunable Heterojunctions in Organic and Colloidal Quantum Dot Photovoltaics

Yufei Zhong[1,2], Ahmad R. Kirmani[2], Xinzheng Lan[3], Joshua Carpenter[4], Annabel Rong-Hui Chew[5], Omar Awartani[4], Liyang Yu[2,6], Muhammad R. Niazi[2], Oleksandr Voznyy[7], Hanlin Hu[2, 8], Guy Olivier Ngongang Ndjawa[2], Max L. Tietze[2, 9], Alberto Salleo[5], Harald Ade[4], Edward H. Sargent[7], Aram Amassian[2, 10]**

[1]School of Materials Science and Engineering (MSE), NingboTech University, No.1 South Qianhu Road, Ningbo 315100, P. R. China.

[2]King Abdullah University of Science and Technology (KAUST), KAUST Solar Center (KSC) and Physical Sciences and Engineering Division, Thuwal, 23955-6900, Saudi Arabia

[3]School of Optical and Electronic Information and Wuhan National Laboratory for Optoelectronics (WNLO), Huazhong University of Science and Technology, Wuhan, Hubei 430074, P. R. China

[4]Department of Physics, and Organic and Carbon Electronics Laboratories (ORaCEL), North Carolina State University, Raleigh, NC, 27695 USA

[5]Department of Materials Science and Engineering, Stanford University, Stanford, CA, USA

[6]School of Chemical Engineering, Sichuan University, Chengdu 610064, P. R. China

[7]Department of Electrical and Computer Engineering, University of Toronto, 10 King's College Road, Toronto, Ontario, M5S 3G4, Canada

[8]Hoffman Institute of Advanced Materials, Shenzhen Polytechnic, 7098 Liuxian Boulevard, Shenzhen 518055, P. R. China

[9]Centre for Membrane Separations, Adsorption, Catalysis and Spectroscopy for Sustainable Solutions (cMACS), University of Leuven, Celestijnenlaan 200F, box 2454, 3001 Leuven, Belgium

[10]Department of Materials Science and Engineering, and Organic and Carbon Electronic Laboratories (ORaCEL), North Carolina State University, Raleigh, NC, 27695 USA.

Author information

Corresponding Author

*Yufei Zhong E-mail: yufei.zhong@nit.zju.edu.cn

*Aram Amassian E-mail: aamassi@ncsu.edu

Abstract

Conjugated polymers are widely used as photoactive and transport layers in organic and hybrid photovoltaics (PV), where the energetics of polymers are a key design criterion. Here, we show that significant variations in terminal molecular ordering between top and bottom surfaces of a wide range of conjugated polymer films, can result in sizable interfacial ionization energy (IE) differences by as much as 0.33 eV, which has significant impact on organic and hybrid PV devices. Such tunability is surprisingly seen even in nominally amorphous polymers. We devise a strategy leveraging wet and dry laminations to form donor-acceptor planar heterojunction (PHJ) devices using exposed and buried surfaces of donor polymers and demonstrate meaningful influence over the open circuit voltage (V_{OC}) by up to 0.32 V. We use this insight to devise a controlled intermixing approach which yields superior V_{OC} and J_{SC} to conventional bulk heterojunction devices by leveraging the disordered interface to maximize V_{OC} and the greater aggregation of the donor to increase the J_{SC}. We go on to demonstrate how judicious control of polymer surface IE benefits charge extraction in colloidal quantum dot PV devices in the role of hole transport layers. Our results show that polymer interfacial and bulk properties are both critical to the functionality of optoelectronic devices and should both be given prime consideration when designing heterojunction devices.

1. Introduction

Conjugated polymers have been broadly applied in organic electronics as channel layers in field-effect transistors, photoactive layers in solar cells, hole or electron transporting layers, as well as transparent conducting layers in organic and hybrid optoelectronic devices.[1-5] The uses of conjugated materials demands increasingly precise and reproducible control over their self-

assembly and structure through molecular design and processing. The orientation of the polymer backbone can significantly impact the electronic properties and lead to anisotropic charge transport.[6] Additionally, the semi-crystallinity of polymers influences the degree/size of aggregation, and therefore impacts photo-physical processes such as charge separation and recombination critically in organic photovoltaics (OPV).[7-10]

During solution processing of semi-crystalline polymers, nucleation triggers the formation of crystalline domains, initially at the liquid-air interface.[11-16] By controlling the drying kinetics, the desirable aggregation state and texture of the polymer may be achieved, but the bulk and buried interface may aggregate differently under such circumstances.[11, 16, 17] Such aggregation behavior may be characterized by widely used bulk measurement methods such as absorption (vibronic features, blue/red-shift of absorption peaks), cyclic voltammetry (CV, energy levels) and X-ray characterization methods (order and orientation). The material properties revealed by these measurements are usually used to explain the differences observed in device performance, but they are often bulk-related properties and assumed to be uniform across the entire film. However, the presumed homogeneity is not realistic and may not extend to the free surface or the buried interface.[18, 19] For instance, the donor (D)/acceptor (A) interface in organic photovoltaics (OPVs) dominates device performance by hosting charge separation and recombination processes. Even changing one monolayer at this interface has been shown to significantly affect device performance.[20-22] In addition, polymer hole transporting layers (HTLs) must achieve energy level alignment with the active layer in colloidal quantum dot (CQD) and halide perovskite PV devices to promote collection of charges and suppression of bimolecular recombination near the electrode.[23, 24] We therefore take the view that bulk properties can be misleading indicators or predictors of photo-physical processes or device figures of merit.

In this work, we show the energetics and properties of the free and buried interfaces of the polymer film dominate the properties of functional interfaces in optoelectronic devices. We

leverage the tunability of local aggregation and order in top/bottom surfaces of conjugated polymer films to create nominally sharp interfaces with tuned polymer energetics and thus create tailored heterojunction organic photovoltaic devices with tunable V_{OC} and V_{OC} loss, as well as colloidal quantum dot solar cells with enhanced charge extraction behavior. For instance, using the top and bottom surfaces of the same conjugated polymer film with the help of lamination methods,[5, 25-27] we demonstrate planar heterojunction (PHJ) OPV devices with V_{OC} as low as 0.29 V for an ordered polymer at the heterojunction to a high of 0.61 V for a disordered polymer at the heterojunction, while the disordered and mixed heterojunction further increases the V_{OC} to 0.71V. We assess the properties of the free and buried interfaces of a wide range of polymers and successfully classify those exhibiting significant differences between the free and buried surfaces and those exhibiting small or no such differences based on the polymer's ability to aggregate in the solid state. We further exploit the tunability of surfaces of aggregating polymers to create bespoke interfaces in HTLs in modern CQD PVs. In doing so, we fine-tune the interfacial and heterojunction properties, recombination and extraction behaviors, and effect significant change in device figures of merit by using a different surface of the same polymer film exhibiting a different aggregation/order state. The direct linkage between V_{OC} of PHJ devices and the degree of order of the polymer at nominally sharp D/A interfaces as opposed to bulk polymer properties highlights the importance of considering polymer surface and interface states when designing and fabricating conjugated polymers and optoelectronic devices.

2. Results and Discussion

2.1 Aggregation of Top vs. Buried Surfaces: Tunable Energetics

To investigate interfaces in semi-crystalline conjugated polymer films and devices, we first assess the aggregation behavior of the archetypal and well-studied high molecular weight (Mw, 50-100K) regioregular poly(3-hexylthiophene-2,5-diyl) (P3HT). Vertically inhomogeneous aggregation has been reported in this instance and is believed to be induced by sequential

aggregation resulting in stratification during solution processing in many types of materials,[11, 15-17] and derives from the formation of a thin skin layer at the liquid/air (L/A) interface where solvent evaporates and the solute tends to accumulate, as depicted in Fig. 1a.[28-31] Upon drying, this skin layer is expected to remain and defines the surface termination of the polymer film (top surface). In contrast, the aggregation state of the remaining polymer solute defines the buried solid/liquid (S/L) interface (bottom surface), which may be tuned by the rate of evaporation of the solution which controls the time remaining for self-assembly.[32-34]

Following this logic, we prepared P3HT films using three different solvents with increasing boiling points (BP) and vapor pressures (VP) decreasing by two orders of magnitude, namely chloroform (CF; BP = 61.2°C; VP = 197 mm Hg at 25°C), chlorobenzene (CB; BP = 131.6°C; VP = 12 mm Hg at 25°C) and dichlorobenzene (DCB; BP = 180°C; VP = 1.36 mm Hg at 25°C) to create films with large (CF), intermediate (CB) and low (DCB) inhomogeneity.[35, 36] To assess the ability to tune interfacial order and associated energetics and other properties, we sought to isolate the buried (bottom) interface for characterization. Lamination is a widely used technique to prepare layered structures, we here utilized this approach to deliberately access buried interfaces for in-depth characterization or to flip polymer films and utilize their exposed surface as functional interface in various (opto)electronic device geometries.[18, 25-27, 37-39] To flip the film, the glass/polymer substrate was slowly merged into water from one corner of the substate. The edge of the polymer film was pre-scratched to expose the interface between the polymer and glass so as to allow water ingress at the interface, resulting in delamination of the film. The target substrate is then gently placed either above or below the film floating on water, carefully attaching to the film from one corner, until the whole film is attached or laminated onto the substrate, as briefly depicted in Fig. S1 in supporting information (SI).

We then performed ultraviolet photoemission spectroscopy (UPS) to analyze the ionization energy (IE) of top and bottom surfaces of P3HT films processed using the above three solvents. The UPS data is taken by measuring three samples, and three different sample areas are checked

for each sample to obtain the average IE and standard deviation. The fitting of data is done by the cross point of baseline and onset curve. We use a low measurement intensity to avoid degradation of polymer film. We also change the intensity for the measurement to exclude any charging effect. The fact that the good agreement between our data and reported literature also validate the reliability of our UPS results.[40-42] As shown in Fig. 1b, the top panel confirms negligible change of the photoelectron energy cut-off region for top surfaces of P3HT films prepared by the different solvents, since all three systems allow the skin layer to form (data of Fermi region is provided in Fig. S2). In contrast, the bottom panel clearly shows a dramatic shift of the cut-off towards high energy with decreasing evaporation rate (increasing BP) of solvents. The summary of UPS data in provided in Table 1. This demonstrates that the solvent evaporation dynamics strongly affect the energetics of the buried interface. Additionally, all three top surfaces exhibit cut-offs at higher energy position compared to their bottom counterparts. This is ascribed to a surface dipole moment formation on the top surface of P3HT films regardless of solvent used. The bottom surface, however, does not exhibit a dipole moment with CF and the IE becomes shallower upon higher BP of the solvent due to the above-mentioned dipole moment formation. According to previous reports, a surface dipole moment exists when polymer backbone is aligned preferentially with an edge-on orientation.[43] UPS results here suggest top surfaces may have a preferred edge-on orientation or, alternatively, a more ordered and textured packing of polymer chains, which induces the aforementioned dipole moment. The bottom surfaces, however, do not exhibit this, indicating they either do not tend to be edge-on orientated or the packing of polymer chains is considerably less ordered due to quenching, but may gradually increase in order with increasing solvent BP, as will be confirmed below. Finally, we compare the variation of IE ranges from 4.56 to 4.65 eV (top surface) and from 4.66 to 4.89 eV (bottom surface) in this work to values reported in the literature. Although the reported IE is only measured for top surfaces, we did find the IE of P3HT also differs a lot depending on the processing/post processing conditions. The large variation between reported

IE in P3HT processed by CF (4.54 eV),[40] CB (4.54 eV, 4.65eV, 4.7 eV),[40-42] DCB (4.67 eV)[44] and post annealing (4.2 eV)[45] confirms the IE could be significantly affected by the aggregation of polymer. The similarity between some of these reported values and our data validates our above discussion that inhomogeneous aggregation exists in polymer films and also indicates controlled processing condition could lead us towards designated IE of the film.

To verify the above hypothesis of surface orientation, we carried out near-edge X-ray absorption fine structure (NEXAFS) measurements. As selectively shown in Fig. 1c, the π area in the bottom surface (CB as solvent) has very little dependence on the incidence angle while the top surface shows increased signal with larger incidence angle. As a result, the values of dichroic ratio (DR) calculated are -0.10 and 0.27 for bottom and top surfaces, respectively. Note that DR is related to the azimuthal mean orientation of the orientation distribution with its incident angle, defined as follow:

$$\mathrm{DR} = \frac{\mathrm{I}(90°)-\mathrm{I}(0°)}{\mathrm{I}(90°)+\mathrm{I}(0°)} \quad (1)$$

where I is the orientation distribution, defined as:

$$\mathrm{I} = \mathrm{A} * [\frac{\mathrm{P}}{3}\left(1 + \frac{1}{2}\{3\cos^2\theta - 1\}\{3\cos^2\alpha - 1\}\right) + \frac{(1-\mathrm{P})}{2}\sin^2\alpha] \quad (2)$$

where A is constant, P is polarization factor of beamline, θ is incident angle, α is angle of π* orbital relative o substrate normal. Because DR can vary from positive value for a horizontal orbital (edge-on) to negative value for a vertical orbital (face-on), we therefore identify a more edge-on orientated top surface compared to slightly face-on orientated or non-orientated bottom surface. Furthermore, the inset in Fig. 1c shows the DR value for bottom surface of P3HT samples prepared by different solvents. We clearly observe the transition of bottom surface from face-on orientation towards slightly edge-on orientation (DR value from -0.20 to 0.07) when prolonging the time for self-assembly (higher BP solvents). This is reasonable due to the lower energetic state of P3HT is edge-on, meaning longer time for self-assembly gives more edge-on orientation in the film.[46] NEXAFS results here agree with UPS data, confirming our

hypothesis that the skin layer formation during stratification locks the aggregation state (solvents have little impact on top surface since it's already ordered enough with a preferred edge-on orientation) of polymer chains near top surface of polymer film while that in bottom surface could be altered by the choice of the solvent. The above results clearly demonstrate existence of inhomogeneous aggregation states between the surface and bulk of the polymer films with a strong dependence on the solvent BP.

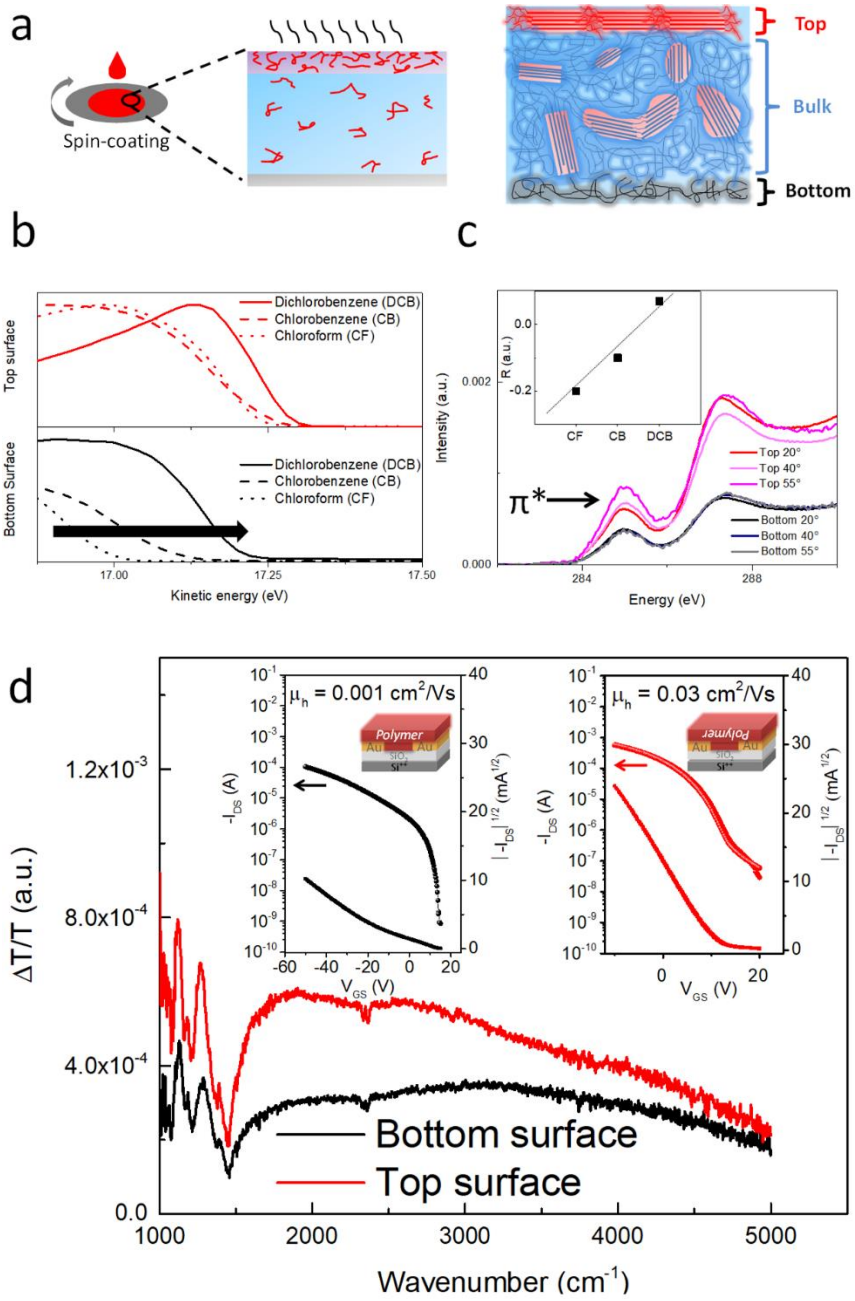

Fig. 1. a. Illustration of stratification process during solution process of polymer films. The skin layer formation at air/solution interface induces different aggregation states of polymer chains in top/bottom surface of polymer film after drying. b. Shift of secondary electron cut-off measured by UPS at top (red) and

bottom (black) surface of P3HT samples processed by different solvents. c. NEXAFS results of top/bottom surface of P3HT samples processed by CB. The inset shows R values of bottom surface of P3HT samples processed by different solvents. d. charge modulation spectroscopy (CMS) results of top/bottom surface of P3HT samples processed by CB. The inset shows OFET device results using top/bottom surface of P3HT films processed by CB to construct interfaces.

Table 1. UPS results of top/bottom surfaces of P3HT films. Average values are obtained by measuring three samples, and three different sample areas are checked in each measured sample so as to get average value and standard deviation.

Solvent	Cut-off/eV (top)	Cut-off/eV (bottom)	HOMO onset/eV (top)	HOMO onset/eV (bottom)	Fermi level/eV (top)	Fermi level/eV (bottom)	Dipole moment/eV	IE/eV (top)	IE/eV (bottom)
CF	17.22±0.02	16.94±0.02	0.67±0.02	0.63±0.02	3.99±0.02	4.22±0.02	0.24±0.02	4.65±0.02	4.89±0.02
CB	17.23±0.01	17.11±0.01	0.68±0.01	0.70±0.01	3.97±0.01	4.12±0.01	0.14±0.01	4.65±0.01	4.79±0.01
DCB	17.28±0.01	17.18±0.01	0.64±0.01	0.64±0.01	3.92±0.01	4.02±0.01	0.10±0.01	4.56±0.01	4.66±0.01

Apart from above discussion, molecular conformation and orientation are two among several important characteristics differentiating the aggregation states at the top and bottom surfaces of the polymer films we have studied. Additional factors include the degree of molecular coupling, backbone planarity and chain entanglement, all of which can influence the interpretation of the above results (UPS result in particular). However, these factors are difficult to differentiate or decouple using conventional characterization techniques. For this purpose, we use surface-sensitive charge modulation spectroscopy (CMS) to assess the overall difference in inter/intra-chain coupling in top and bottom surfaces of P3HT films. CMS measures polaron absorption and differentiates single chain and 2D delocalized polarons.[47] In the measurement, modulated polarons accumulate at the dielectric-P3HT interface, allowing one surface to be studied over the other by careful placement of the P3HT layer. As shown in Fig. 1d, the top surface of P3HT clearly shows a stronger signal (2000 cm^{-1}) than its bottom surface when processed using CF.

The enhancement in CMS is attributed to the polaron oscillator strength, which is a function of the inter-chain and intra-chain disorder (coupling) in the polymer. Such enhancement suggests higher order (coupling) of P3HT in its top surface. Furthermore, the blue shift of the main peak indicates greater single-chain character for the bottom surface as compared to the top surface, meaning the backbone of P3HT near the bottom is less planar and less aggregated. These results generally agree with UPS and NEXAFS data which, overall, show stronger coupling of molecules and better packing of chains in the top surface of the polymer film as compared to its bottom surface.

We then fabricated bottom-gate bottom-contact OFETs using both top and bottom surfaces of P3HT films to construct the semiconductor-dielectric (S-D) interface since only ~1-2 nm interface region is responsible for carrier transport in the channel. We thus utilize OFETs as a device-based, sensitive, but indirect diagnostic tool of differences in local and long range in-plane order at the top and bottom surfaces of the polymer film. As shown in the inset of Fig. 1d, devices (processed by CB) using the top surface as S-D interface show a ~30x increase in hole mobility compared to devices using the bottom surface as channel material. This result provides further confirmation of improved polymer ordering at surface termination leading to considerably faster carrier transport than at the buried interface, in agreement with previous observations.[26]

Next step, we carry out grazing incidence wide angle X-ray scattering (GIWAXS) measurement to probe crystalline order more directly, albeit with less depth resolution. As shown in Fig. S3 and Fig. S4 we have conducted GIWAXS on top/bottom surface of P3HT films with incident angle of 0.25° and 0.05°, respectively. The former angle will allow the X-rays to penetrate the whole film (40-50 nm) while the latter can induce total reflection of X-ray where an evanescent wave allows us to probe approximately 5-10 nm region near the polymer surface. As known from the laws of classical electrodynamics, this shallow angle of incidence below the critical angle of P3HT for X-ray energy used in these measurements (0.10°) will result in an

exponentially decaying electromagnetic field below a few nanometers from the top surface, making this incidence angle highly surface sensitive. It is clear that no difference is observed at 0.25° incident angle due to the identical bulk properties of the same film. However, there is a clear orientational transition from face-on towards edge-on in top surface region under 0.05° incident angle when switching processing solvent from CF to CB. Similarly, such transition also takes place in bottom surface region when switching the solvent from CB to DCB. These results suggest the time for self-assembly strongly impacts the bottom surface region since it needs more time to transit from face-on to edge-on (due to lower ordering) compared to top surface region because of aforementioned drying kinetics. Additionally, we selectively show here the in-plane and out-of-plane sector cut of P3HT processed by CB in Fig. S5. Top surface region (incident angle 0.05°) clearly exhibits strong higher-order lamellar features (100, 200, 300) than its bottom counterpart. Furthermore, a pronounced π-π stacking (010) also confirms top surface is highly ordered/textured. These results extend our above conclusion of highly ordered top surface (~1 nm) towards a slightly deeper region (~5-10 nm) near the top surface. Lastly, above results also reveal the difference between general bulk properties and surface/interface region properties, cautioning us to focus on the difference in local ordering in near-surface regions of the film when forming functional interfaces in (opto)electronics.

2.2. Classifying Modern Conjugated Polymers by Tunability of Surface Ionization Energy

To generalize the above phenomenon from reference poly(3-hexylthiophene-2,5-diyl) (P3HT), we have expanded our analysis to several other donor polymers , including poly(2,5-bis(3-hexadecylthiophen-2-yl)thieno[3,2-b]thiophene (pBTTT), poly[4,8-bis-(2-ethyl-hexyl-thiophene-5-yl)-benzo[1,2-b:4,5-b]dithiophene-2,6-diyl]-alt-[2-(2-ethyl-hexanoyl)-thieno[3,4-b]thiophen-4,6-diyl] (PBDTTT-C-T), Poly[(5,6-difluoro-2,1,3-benzothiadiazol-4,7-diyl)-alt-(3,3’’’-di(2-octyldodecyl)-2,2’;5’,2’’;5’’,2’’’-quaterthiophen-5,5’’’-diyl)] (PffBT4T-2OD), Poly[4,8-bis(5-(2-ethylhexyl)thiophen-2-yl)benzo[1,2-b;4,5-b']dithiophene-2,6-diyl-alt-(4-(2-ethylhexyl)-3-fluorothieno[3,4-b]thiophene-)-2-carboxylate-2-6-diyl)] (PCE10) and Poly

[[4,8-bis[(2-ethylhexyl)oxy]benzo[1,2-b:4,5-b']dithiophene-2,6-diyl][3-fluoro-2-[(2-ethylhexyl)carbonyl]thieno[3,4-b]thiophenediyl]] (PTB7) (chemical structures shown in Fig. 2), selecting ones which are known to crystallize, such as pBTTT, as well as others like PTB7, which do not crystallize at all. For the purpose of this comparison, all films were processed using CB as solvent, achieving nominally similar drying dynamics, to evaluate the comparative ability to achieve distinctive free and buried bottom surface properties. By applying our lamination approach, we then evaluate the IE of all polymer films' top and bottom surfaces, including P3HT processed in all three solvents. The results are obtained using a similar surface-sensitive method, namely photoelectron spectroscopy in air (PESA). PESA spectra are shown in Fig. S6. The resolution of PESA is in general higher than UPS. We also performed the measurement on 3 different samples using 3 different probing areas on each sample to obtain average values of IE for each material. The IE was obtained by the cross-point of the baseline and onset of curves for each measurement. Fig. 2 summarizes the IE for all polymers. It is clearly shown that P3HT and pBTTT are part of a class of highly energy-tunable polymers with ΔIE (difference between IE_{bottom} and IE_{top}) as high as 0.33 eV, while a second group of polymers (PCE10, PffBT4T-2OD and PBDTTT-C-T) shows differences that are small (ΔIE ~0.1 eV) but consistent, measurable and non-negligible, with one polymer (PTB7) showing no measurable difference between energetics of the top and bottom surfaces (ΔIE ~0).

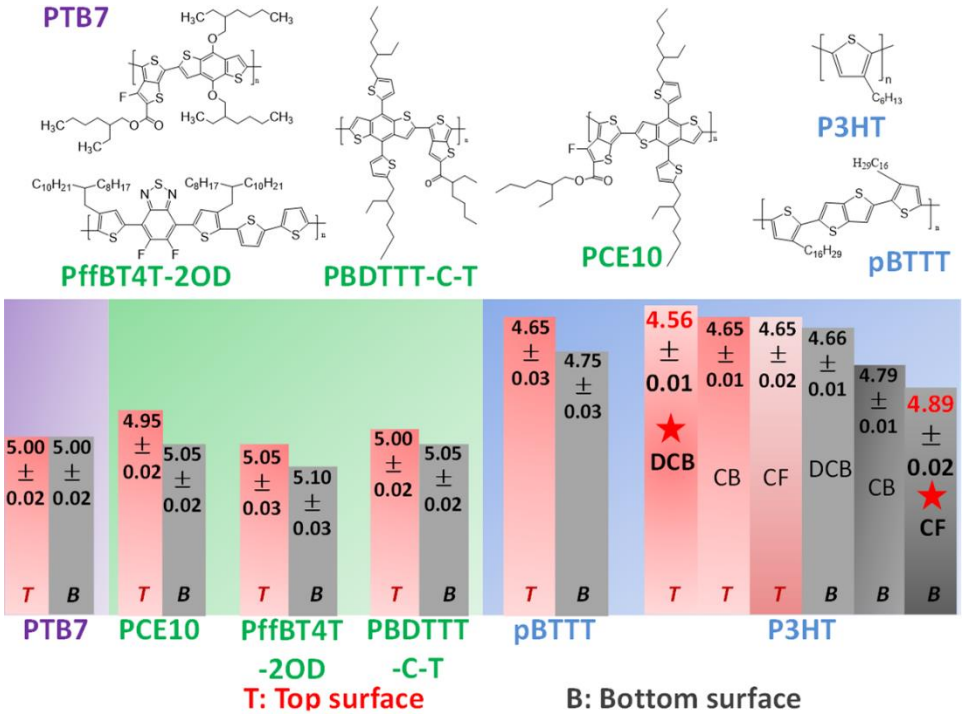

Fig. 2. Average IE (eV) with standard deviation from PESA for top/bottom surfaces in different polymers processed by CB. The polymers are simply categorized into three kinds: large (P3HT, pBTTT), medium (PCE10, PffBT4T-2OD and PBDTTT-C-T), and negligible (PTB7) ΔIE of top and bottom surfaces. P3HT possesses the largest difference ranging from 4.56 to 4.89 eV among surfaces processed by different solvents.

2.3. Organic Photovoltaics with Tunable Heterjunctions

2.3.1 Planar heterojunction (PHJ) photovoltaics with tunable interfacial energetics

Given the tunability of IE by up to 0.33 eV (in the case of P3HT), we possess a means of tuning the interfacial energetics and polymer order, albeit the latter only in the case of highly aggregating polymers. We can now turn to constructing model D/A interfaces in the context of planar heterojunction (PHJ, also known as bilayer) OPV devices, focusing first on P3HT/PCBM bilayers, to reveal the relationship between interfacial energetics, order and open circuit voltage (V_{OC}) of OPV devices in the context of nominally sharp interfaces (formed through lamination without annealing), then generalizing to other donor and acceptor systems. The exact aggregation state of the polymer near the D/A interface is in general unclear due to the various mixing/demixing scenarios of D and A molecules in a BHJ and is nearly impossible to disentangle within BHJ devices.[48-50] Fig. 3a illustrates interfaces that may exist within BHJs, namely ordered-ordered D/A interfaces, disordered-disordered D/A interfaces and

intermediates thereof, such as ordered-disordered and disordered-ordered D-A interfaces, and the mixed phase itself.[8, 51] The overall V_{OC} of the device therefore is a weighted combination of local or individual energy of charge transfer state (E_{CT}) and thus V_{OC} contributions by these different charge generation pathways. The conventional bulk characterization of BHJ OPVs to date using absorption, global energy levels and even the lowest E_{CT} do not reflect the complete operational behavior of the ensemble of D/A interfaces which together determine the V_{OC}.[50, 52] These observations are in agreement with previous reports showing the coexistence of ordered and disordered phases in the film which together impact molecular energy level shifts and thus reflected in interfacial charge transfer (CT) states.[53] The corresponding E_{CT} and V_{OC} are therefore weighted contributions from different morphologies, such as ordered/disordered interfaces.[53] In this sense, model PHJ interfaces prepared by lamination can be very powerful instruments to disentangle the contributions of different interfaces in a BHJ by reducing these various types of interfaces to accessible systems that may be isolated and investigated.

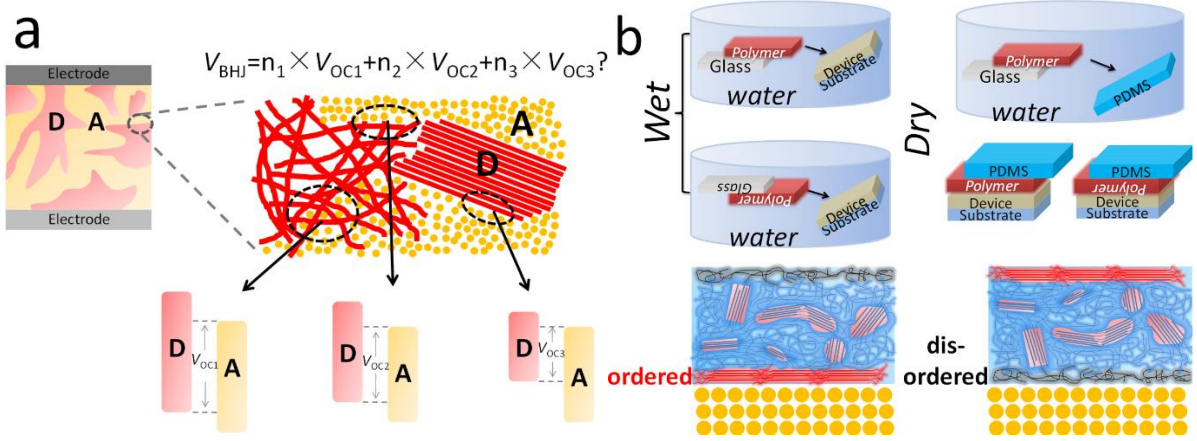

Fig. 3. a. Conceptual illustration of interfaces in bulk-heterojunction with their corresponding V_{OC}. The V_{BHJ} therefore is a weighted combination of these V_{OC}s. Schematic volumetric fractions of these V_{OC}s are listed as n_1, n_2, and n_3. b. Lamination methods (top left: wet method; top right: dry method) making planar heterojunction using top/bottom surface of polymer films. Bottom cartoon shows different aggregation state at top/bottom surface of polymer films can induce different interfacial energetics, thus V_{OC}.

Similar to how we flip the pristine polymer film, the preparation of bilayer also involves de-laminating of the film in water. The target substrate consists of glass/ITO/ZnO/acceptor, shown as substrate/device in Fig. 3b, is then slowly attaching from one side (top/bottom) of the polymer until full lamination of polymer atop the target substrate/device.[20, 21, 50, 52, 54-56] Such

wet method involves merging the whole substrate/device in water, which might in some cases degrade the device such as water sensitive quantum dots. We therefore also use another dry lamination method shown in upper right of Fig. 3b. Such processes similarly delaminate the polymer film in water, but use a PDMS stamp to transfer and release the film onto target water sensitive device. The PDMS stamp is placed to attach the polymer film from one corner until full lamination of film on PDMS. The PDMS/polymer is then placed upside down onto target device and softly stress to de-laminate the film onto the device. After fabrication of bilayer, additional thermal annealing of PHJs can subsequently be used to induce acceptor diffusion into the donor layer in order to transform the bilayer into a BHJ-like film or to one where the interface is no longer abrupted and therefore evaluate the influence of intermixing.[27, 57]

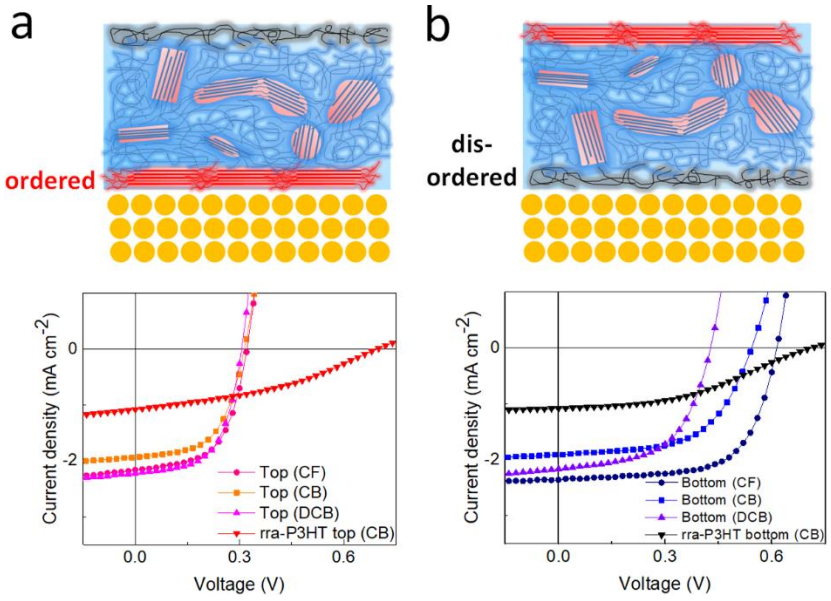

Fig. 4. a. *J-V* curves of bilayer OPV consist of top surface of P3HT processed with different solvents as interface, top surface of rra-P3HT processed by CB is also used as interface for comparison. b. *J-V* curves of bilayer OPV consist of bottom surface of P3HT processed with different solvents as interface, bottom surface of rra-P3HT processed by CB is also used as interface for comparison. The thickness for both polymer and fullerene layer are around 40 nm.

We have here used lamination to recreate different model D/A interfaces and assess the V_{OC} in PHJ devices with nominally sharp interfaces. *J-V* curves of PHJ P3HT/PCBM devices using the top/bottom surfaces of P3HT films processed by different solvents as planar D/A interface are shown in Fig. 4a and 4b (see device figures of merit in Table S1). We observe that V_{OC} is very sensitive to the state of the P3HT surface and that it is significantly and directly impacted

by IE (Table 1) of the P3HT surface used. V_{OC} in devices using the top surface of P3HT as the interface is consistently lower (V_{OC}≈0.3 V) and nearly equal across all three solvents, in agreement with UPS measurements revealing a shallow IE at top surfaces due to the presence of a surface dipole which we link to improved ordering, and is consistent with other measurements highlighting the similarity of the top surfaces of P3HT films irrespective of the solvent used. In contrast, the impact of the solvent choice and polymer order is clearly observed when PHJ devices are fabricated using the bottom surface of P3HT films as their D/A interface. V_{OC} of these devices gradually decrease from 0.61 V (CF) to 0.56 V (CB) to 0.44 V (DCB) with decreasing evaporation rate of solvent and increasing order at the interface, which also leads to dipole moment formation, as evidenced by our UPS data. We note that the most disordered interface yields the highest V_{OC} (0.61 eV). It is common that different values of V_{OC} could be found in P3HT:PCBM blends. V_{OC} of P3HT:PCBM ranges from 0.5 to 0.65 V depending on processing condition/annealing/molecular weight and thus morphology in these blends.[58-63] The V_{OC} obtained in device with disordered interface here is in good agreement with that generally observed in reported literatures, validating such interface is similar compared to those reported in BHJ to date. We also note such disordered interface yields high V_{OC} appears to be somewhat counter-intuitive. On one hand, disordered interfaces give deeper IE of a polymer thus larger difference between HOMO of the donor and the LUMO of the acceptor, enlarging V_{OC}; on the other hand, it should also decrease the delocalization of charges causing energy loss through recombination. These factors should drive V_{OC} of the device oppositely. The results we present above clearly show that the interfacial energetics play the dominant role in determining V_{OC}. Furthermore, it is important to note that our method produces disorder at the buried interface rather than in the bulk of the film, which is an important distinction to avoid recombination. The presence of order in the bulk allows both exciton diffusion and charge transport to and away from the disordered interfacial region. Such a benefit cannot be expected when using an amorphous polymer such as regiorandom (rra-) P3HT which exhibits both low exciton diffusion

as well as low carrier mobility.[64-66] In other words, the impact of disorder-induced shift of IE of a polymer outcompetes that of disorder-induced energy loss when these effects are confined to the interface, leading to the higher V_{OC} in the device with the most-disordered bottom layer (see more discussion of energy loss below). We found no difference in the IE of the top and buried surfaces of rra-P3HT films as these films are uniformly disordered. Fig. 4a and 4b show PHJ devices of rra-P3HT/PCBM using both top and buried surfaces using CB solvent and revealing identical V_{OC} (0.71V) for both surfaces, a value slightly larger but similar to the P3HT buried interface processed with CF, indicating further reduction in interfacial order. Finally, we generalize the above conclusions by combining P3HT, first, with other acceptors, such as Bis-PCBM and a non-fullerene acceptor (5Z,5'Z)-5,5'-((7,7'-(4,4,9,9-tetraoctyl-4,9-dihydro-s-indaceno[1,2-b:5,6-b']dithiophene-2,7-diyl)bis(benzo[c][1,2,5]thiadiazole-7,4-diyl))bis(methanylylidene))bis(3-ethyl-2-thioxothiazolidin-4-one) (O-IDTBR), and ZnO inorganic layer. Similar V_{OC} differences are observed, confirming the dominant role of energetics induced by interfacial ordering and interfacial energetics (see data and detail discussion in Fig. S7 and figure of merit in Table S2). As expected, we note that the efficiency of PHJ devices is considerably lower than that of BHJ films (less than 1%) and consistent with previous reports of PHJ devices.[21, 27] However, the main purpose of PHJ devices is to investigate the influence of interfacial structure and energy on the V_{OC}[21, 27] and to reveal which interfaces dominate the V_{OC} of BHJ devices.

2.3.2 From model PHJs to BHJs with enhanced V_{OC} and J_{SC} via Interdiffusion

The above results shows that V_{OC} of heterojunction devices is a very sensitive indicator of interfacial aggregation state of the donor polymer (and thus interfacial energetics), and can therefore reveal more about interfaces within the BHJ itself and how to improve these to maximize the V_{OC}. As shown in Fig. 5a, the as-cast P3HT:PCBM BHJ has a high V_{OC} of 0.72 V which decreases to 0.6 V upon annealing, caused by aggregation and phase separation, as

depicted on the upper right (figures of merit shown in Table S3). The device V_{OC} prior to annealing is closest to that of rra-P3HT based PHJ device (0.71 V) and considerably higher than the P3HT (CF)-PCBM interface created with the buried interface (0.61 V), which is in fact closer to the V_{OC} of the annealed BHJ film. The considerably lower V_{OC} (0.3 V) of the ordered-ordered PHJ P3HT/PCBM devices indicates that such interfaces are not the main channels for charge generation in BHJ devices. Instead, there appears to be a significant contribution of disordered P3HT at interfaces, perhaps due to an intermixed phase where intermolecular coupling is reduced, as previously proposed by several groups.[67, 68]

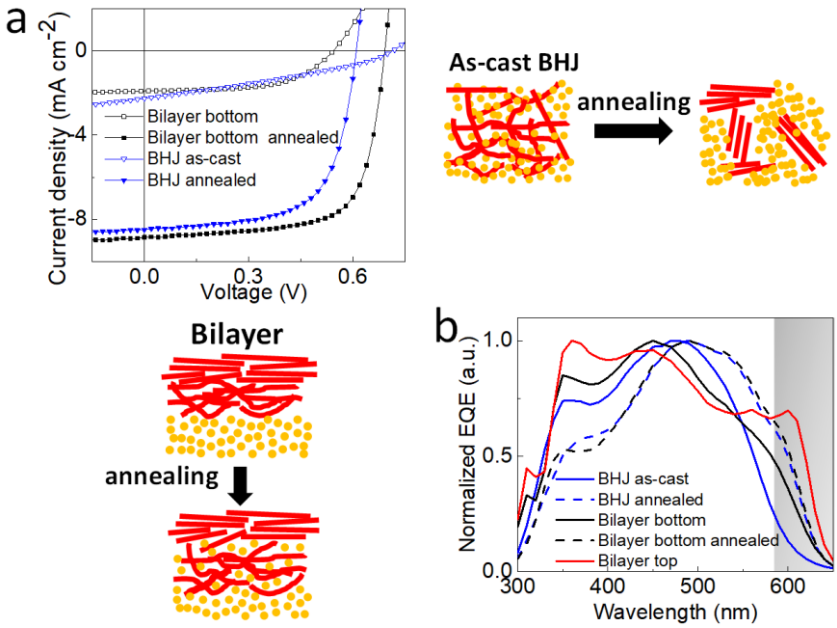

Fig. 5. a. *J-V* curves of P3HT:PCBM bilayer (P3HT bottom surface as interface) and BHJ devices before and after annealing. Cartoon on the upper right shows annealing induced phase separation in BHJ and cartoon on bottom left shows annealing induced phase mixing in bilayer by PCBM diffusion, creating a BHJ like interfacial area. b. EQE response of bilayer and BHJ before and after annealing. The gray zone indicates the enhanced 0-0 transition in device with different interfaces.

We recall that in a BHJ layer the P3HT is vitrified by the presence of the acceptor and its disorder both in the bulk and interfacial regions explains the considerably higher V_{OC} achieved in such devices as compared to PHJ devices of ordered interfaces, as well as limited order achieved in the bulk.[69] We therefore annealed the PHJ device based on the disordered interface (bottom left in Fig. 5) to induce diffusion of PCBM and intermixing with P3HT. However, the bulk order of P3HT is pre-formed prior to lamination and annealing and is not lost through intermixing In doing so, we observe a sharp increase in J_{SC} (*J-V* curves in Fig. 5a) due to

enlarged D/A interfacial area collecting and separating more excitons. We also find a higher V_{OC} of 0.68 V, larger by 0.08 V compared to the annealed BHJ (0.6 V), leading to an overall efficiency over 4%. This efficiency is much higher than previously reported annealed bilayers thanks to the choice of the disordered surface of P3HT as the BHJ interface which leads to the high V_{OC} and J_{SC}.[70] We note the efficiency of 4% obtained with P3HT:PCBM here is far below that in modern OPV devices, date due to the limited light absorption of P3HT and PCBM.[71] We however believe that our methodology which tunes the dominant interfaces responsible for V_{OC} of device should be universally applicable across many modern D/A systems. The high V_{OC} obtained here confirms the aggregation state of P3HT at D/A interfaces in annealed bilayers is predominantly based on disordered polymer-acceptor interfaces compared to BHJ films, while still exhibiting sufficiently ordered and connected polymer domains as required for charge extraction. The fact that the V_{OC} of such annealed PHJ devices approaches that of as-cast BHJs (0.72 V) and surpasses the J_{SC} also validates the above conclusion. These results may have similar implications of morphology control as recently reported stepwise BHJ processing, which also emphasizes the usage of layer-by-layer solution-deposition to achieve a BHJ like interface with a clear vertical phase segregation.[72, 73] Furthermore, we observed significant differences in the shape of external quantum efficiency (EQE) response. As shown in Fig. 5b, normalized EQE spectra show higher response near 610 nm with increasing ordering of P3HT at D/A interface which indicates stronger vibronic feature (0-0 transition) of P3HT. The fact that a bilayer with ordered interface having higher EQE response near 610 nm than that in annealed BHJ also confirms such ordered interface does not dominate charge generation in the BHJ.

2.3.3 Generalizing V_{OC} vs. IE-EA relationship for PHJ devices with sharp D/A interfaces

We now expand PHJ device investigations to the five other polymers studied and classified in the previous section by fabricating polymer-PCBM PHJ devices. The D/PCBM interfacial energetics are summarized in Fig. S8a. The electron affinity (EA) of PCBM here is taken from

our previous report measured by low energy inverse photoemission spectroscopy (LEIPS).[74] We plot V_{OC} of PHJ devices with respect to the IE of the corresponding polymer surfaces in Fig. S8b. Clearly, V_{OC} scales linearly with increased IE of the polymer donor, indicating that this is the primary parameter dictating the V_{OC} for sharp interfaces across different donor polymers. As expected, we find no effect of the surface choices of rra-P3HT (right triangle) and PTB7 (diamond) on V_{OC} in agreement with the absence of IE change. Meanwhile, other polymers exhibiting small differences in IE also exhibit a commensurately small change in V_{OC} (see *J-V* curves and figure of merit in Fig. S9 and Table S4). Additionally, we plot IE_D-EA_A against V_{OC} in Fig. 6. We find similar trend that V_{OC} scales almost linearly with IE-EA. Such results also validate energetics are the main reason for change of V_{OC}. Again, we here only discuss the impact of energetics on V_{OC}. Other factors not included such as local delocalization of charges and D/A coupling might also influence the results in Fig. 6, as evidenced by the deviation from the linear relationship between V_{OC} and IE_D-EA_A.

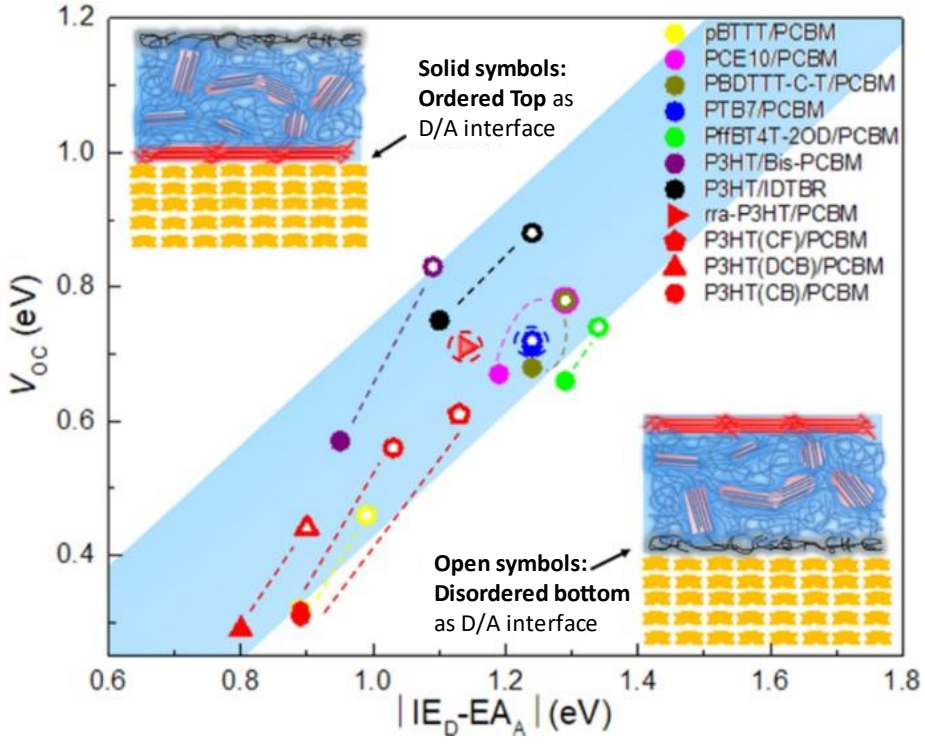

Fig. 6. V_{OC} of nominally sharp polymer/acceptor bilayer with different interfacial states(solid symbol: polymer top surface as interface; open symbol: polymer bottom surface as interface) against the $|IE_D - EA_A|$ (donor: D, acceptor: A) at the interface. The data of same material system is connected by dashed line and system show very little change is marked by dashed circle, the blue shaded area is the arbitrary shading

to indicate a trend. P3HT processed by CF, CB and DCB are shown, while all other polymer and acceptor layers are processed by CB. The LUMOs of Bis-PCBM and IDTBR, and HOMO of rra-P3HT are taken from reported literatures.[75-77]

Note that due to limited D/A interfacial areas in bilayer device, we are not able to detect or measure E_{CT} by using sensitive EQE since the EQE response in sub-bandgap region is too low. We therefore evaluate the influence of interfacial order on V_{OC}loss, by defining it as IE_D-EA_A-qV_{OC}. The V_{OC}loss of analyzed systems is displayed in Fig. S10. Since the main focus of this work is to show the impact of tunable interfacial property induced by aggregation of polymer on corresponding device figure of merit, we here only briefly explain the observed lower V_{OC}loss in devices with disordered bottom surface used as interface by the following two reasons: 1) energy cascade in polymer donor layer induced by a wider bandgap of disordered surface then a lower bandgap of ordered region away from bottom surface/interface;[78] 2) energy gap law which describes a larger interfacial bandgap (thus larger E_{CT}) gives lower (non-radiative) V_{OC}loss.[79] A more detailed discussion is provided in Fig. S10 in SI. Finally, we made a comparison between V_{OC} in our above PHJ and corresponding reported V_{OC} of BHJ in Table S5, in which the latter usually lies in between of top/bottom surface based device of the former. Such results suggest our methodology proposed herein can be generally applied to reveal the nature of distributed interfaces within these modern BHJs.

2.4. Colloidal Quantum Dot Photovoltaics with Tunable HTL-QD Heterojunction

From above results, we clearly identify the significant impact of interfacial aggregation state on charge generation in OPV devices. With that being said, the aggregation state and associated energetic differences between the top/bottom surfaces of polymer films can cause large differences in PV devices when the polymer is used as hole transporting layer (HTL), such as in colloidal quantum dot (CQD) PVs. Selecting polymer HTLs based on energy levels to achieve efficient interfacial charge extraction is a well-known strategy in optoelectronic device optimization. Although traditionally successful in improving p-type charge transport in CQDs

for efficient n-i-p devices, EDT ligands used on p-layer (TBAI) QDs are known to be labile and have been reported to easily detach from the PbS CQD surface, making them susceptible of interacting with metal contacts.[80-82] Due to these inherent issues with EDT ligands, organic semiconductor films have recently attracted interest as potential HTLs, making them particularly attractive to enhance the performance and stability of CQD-PV devices.[83-86]

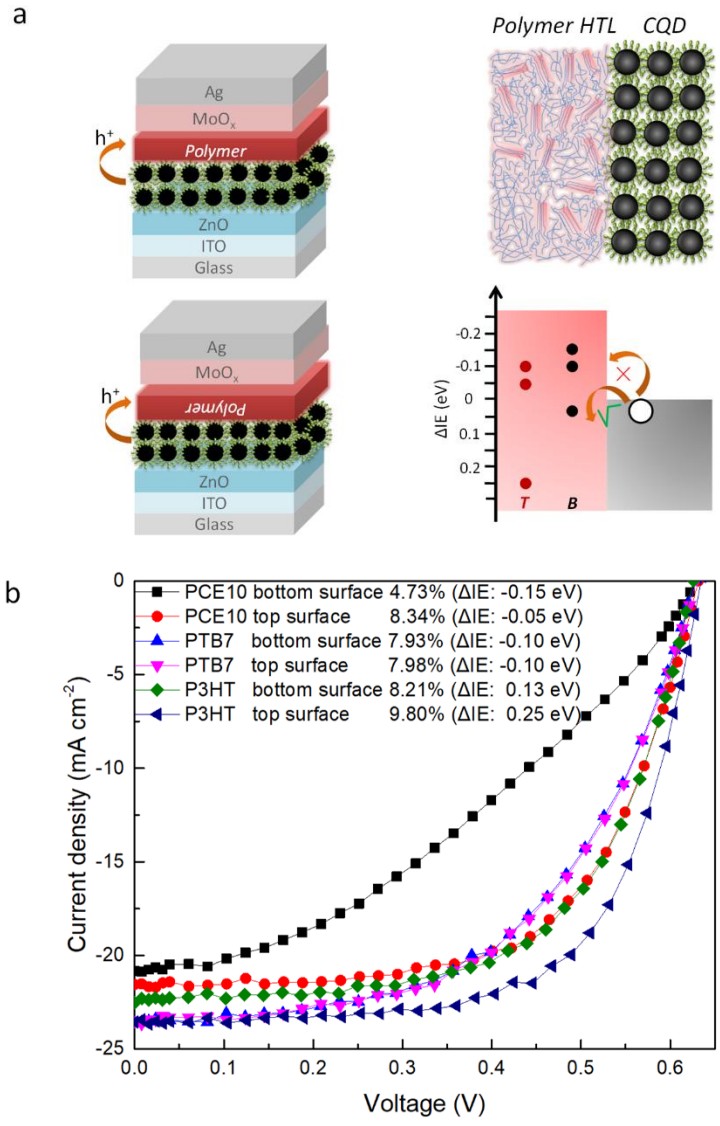

Fig. 7. a. CQD PV using different polymer surfaces as charge (hole) extraction interfaces. The charge injection barrier (bottom right) is defined as the difference of work function (4.9 eV) of CQD and IE of polymers. b. *J-V* curves of CQD PV using different surface of different polymer as charge extraction interfaces.

We herein show that, even with the same polymer film used as HTL, device performance largely depends on the fine-tuned, local interfacial energy of the polymer rather than its bulk or opposite surface energetics. We go on to show that the stability of the CQD-PV devices can be enhanced

by use of polymer HTLs in combination with the EDT-capped CQD layer. To that end, we use different polymers as HTL with their top/bottom surfaces atop the EDT-capped CQD layer. The device architecture is depicted in the left part of Fig. 7a and charge injection barrier at polymer/CQD interface is listed on the bottom right. We clearly see that the device performance is largely determined by the polymer surface used to construct interfaces, as shown in Fig. 7b (see figure of merit in Table S6). Similar to our observation in OPVs, the performance of CQD PV doesn't change much when using PTB7 as HTL due to similar aggregation state in top/bottom surface of PTB7. When PCE10 is used as HTL, the top and bottom surfaces exhibit different injection barriers. However, the FF of devices drop significantly when the barrier increases from -0.05 (top surface) to -0.15 eV (bottom surface). Such results suggest there is a sensitive threshold for injection barrier which jeopardizes charge collection. It also draws the attention of careful characterization of (top/bottom) surface energy levels of HTL when constructing a device's interfaces. The last polymer used here is P3HT, which shows the best efficiency among these HTLs due to good carrier injection at interfaces. Note that similar as in OPV's case, interfacial energetics are not the only factor affecting device performance here. It is possible that other factors such as interfacial trap density can also affect above results. We have done solar cell capacitance simulator (SCAPS) to investigate the impact of interfacial energetics on *J-V* curves of above devices (see Fig. S11). We clearly see the overall trend predicted by such simulation agrees with our device data. The mismatch of IE to achieve best device performance between simulation and experiment however indicate some other factor could be involved in explaining the experimental data, such as aforementioned trap density induced by lower ordering in bottom surface of polymer films. Nevertheless, it is evident that device performance is largely depending on the aggregation state of polymers near the interface. We here use different interfaces, thus energetics, to demonstrate even with the same HTL the interfacial energetics could be much more complicated than simple bulk characterizations, as the bulk property doesn't reflect the property of (top/bottom) surface/interface. We need to

clarify that although large impact of interfacial order on device performance is observed in both CQD PV and aforementioned OPV, the exact working mechanism is however different here. The boost of V_{OC} in OPVs is largely due to a shift of energy levels induced by interfacial local ordering (lower ordering gives higher performance). In CQD PV, on the other hand, the same shift of energy levels didn't affect devices in the same way. As long as the injection barrier is absent, the effect of interfacial energetic is not as large as interfacial traps, thus higher performance of CQD PV is achieved with higher interfacial ordering (lower trap density) in P3HT's case. Finnaly, we also investigated thermal stability of above devices. We found the device with polymer layer capping atop shows stable performance untill 110°C and still functional even at 150°C, whereas the device without polymer layer degrades since 70°C. We explain this phenomenon by the polymer HTL induced prevention of degradation from halide ligands of CQD under high temperature. The data of thermal stability and dependence of device figure of merit upn temperature are provided in Fig. S12 and Fig. S13.

3. Conclusions

In this work, we offer conclusive evidence that conjugated polymer films exhibit different ordering in their top/bottom surfaces, driven by the stratification phenomenon during solution processing. This difference largely depends on the polymer's ability to aggregate in solid state. We generalized this conclusion by testing six commonly used conjugated polymers. The difference of local order of polymer film uncovered here has primary importance in heterojunction based devices since it affects multiple processes such as charge transport, generation and extraction. We utilize these differences effectively in devices ranging from OFETs, to PHJ and BHJ OPVs and CQD PVs, where the polymer is used as channel, photo-active layer and HTL, respectively. Using the knowledge unearthed here, we demonstrated a simple but effective methodology to fabricate PHJ devices with model interfaces allowing us to disentangle the contribution of different types of sharp D/A interfaces in BHJ OPV in terms

of its V_{OC}, which is conventionally not accessible to other characterizations, highlighting the importance of control of interfacial property to reduce energy loss in OPV. We observe a clear relationship between the V_{OC} and energy gap of the D/A materials using these model interfaces and go on to show that different interfacial aggregation states show different V_{OC} in PHJ OPV and therefore the coexistence of different ordered/disordered phase contribute comprehensively in BHJ OPV's V_{OC}. We close our discussion by emphasizing that these unexpected findings could be generally applied beyond the device platforms tested in this work. Interestingly, some of the polymers explored in this work including P3HT have been used as HTLs in some of the high-efficiency and high-stability perovskite solar cells. Lessons from our findings can therefore be helpful to this burgeoning field. In addition, organic/hybrid devices such as LED, thermal electronics, photo detector and sensors can also take advantage of this universal methodology proposed here to further push the limits on their efficiencies by refining their interfaces with these conjugated polymers. Finally, the above knowledge also should provoke a further re-consideration of energetics at organic/organic and organic/inorganic interfaces investigated to date, which roughly considers a homogeneous existence of properties throughout the polymer film.

4. Experimental Details

See Supporting Information (SI).

Supporting Information

See (SI).

Contributions

Y. Zhong carried out film/device fabrication and film/device related characterization. A. R. Kirmani, G. O. N. Ndjawa, M. L. Tietze and Y. Zhong did UPS measurement. M. R. Niazi and Y. Zhong to fabricated FET. A. R. Kirmani, L. Yu, and H. Hu did GIWAXS and GIWAXS analysis. O. Voznyy and E. H. Sargent did SCAPS. X. Lan offered processing recipe for CQD cells. J. Carpenter, O. Awartani and H. Ade did NEXAFS. A.R. Chew and A. Salleo did CMS.

A. Amassian supervised the whole project. All the authors contributed to manuscript preparation.

Notes

The authors declare no competing financial interest.

Acknowledgements

Y. Zhong acknowledges funding supported by Zhejiang Provincial Natural Science Foundation of China under grant No. Y22E021579. H. Ade, J. Carpenter and O. Awartani acknowledge funding supported under ONR N000141512322 and N000141712204.

References

1. S. Fratini, M. Nikolka, A. Salleo, G. Schweicher and H. Sirringhaus, *Nat. Mater.*, 2020, **19**, 491-502.
2. G. P. Kini, S. J. Jeon and D. K. Moon, *Adv. Mater.*, 2020, **32**, 1906175.
3. G.-W. Kim, H. Choi, M. Kim, J. Lee, S. Y. Son and T. Park, *Adv. Energy Mater.*, 2020, **10**, 1903403.
4. V. V. Brus, J. Lee, B. R. Luginbuhl, S.-J. Ko, G. C. Bazan and T.-Q. Nguyen, *Adv. Mater.*, 2019, **31**, 1900904.
5. X. Fan, W. Nie, H. Tsai, N. Wang, H. Huang, Y. Cheng, R. Wen, L. Ma, F. Yan and Y. Xia, *Adv. Sci.*, 2019, **6**, 1900813.
6. S. Qu, Q. Yao, L. Wang, Z. Chen, K. Xu, H. Zeng, W. Shi, T. Zhang, C. Uher and L. Chen, *NPG Asia Mater.*, 2016, **8**, e292-e292.
7. A. C. Jakowetz, M. L. Böhm, J. Zhang, A. Sadhanala, S. Huettner, A. A. Bakulin, A. Rao and R. H. Friend, *J. Am. Chem. Soc.*, 2016, **138**, 11672-11679.
8. M. Scarongella, J. De Jonghe-Risse, E. Buchaca-Domingo, M. Causa', Z. Fei, M. Heeney, J.-E. Moser, N. Stingelin and N. Banerji, *J. Am. Chem. Soc.*, 2015, **137**, 2908-2918.
9. J. R. Tumbleston, B. A. Collins, L. Yang, A. C. Stuart, E. Gann, W. Ma, W. You and H. Ade, *Nat. Photon.*, 2014, **8**, 385-391.
10. B. Kitchen, O. Awartani, R. J. Kline, T. McAfee, H. Ade and B. T. O'Connor, *ACS Appl. Mater. Interfaces*, 2015, **7**, 13208-13216.
11. K. Zhao, O. Wodo, D. Ren, H. U. Khan, M. R. Niazi, H. Hu, M. Abdelsamie, R. Li, E. Q. Li, L. Yu, B. Yan, M. M. Payne, J. Smith, J. E. Anthony, T. D. Anthopoulos, S. T. Thoroddsen, B. Ganapathysubramanian and A. Amassian, *Adv. Funct. Mater.*, 2016, **26**, 1737-1746.
12. Y. Katayama, M. Kalaj, K. S. Barcus and S. M. Cohen, *J. Am. Chem. Soc.*, 2019, **141**, 20000-20003.
13. M. Veschgini, W. Abuillan, S. Inoue, A. Yamamoto, S. Mielke, X. Liu, O. Konovalov, M. P. Krafft and M. Tanaka, *Chemphyschem*, 2017, **18**, 2791-2798.
14. P. G. Argudo, N. Zhang, H. Chen, G. de Miguel, M. T. Martin-Romero, L. Camacho, M. H. Li and J. J. Giner-Casares, *J. Colloid Interface Sci.*, 2021, **596**, 324-331.
15. A. Beaugendre, S. Degoutin, S. Bellayer, C. Pierlot, S. Duquesne, M. Casetta and M. Jimenez, *Prog. Org. Coat.*, 2017, **110**, 210-241.
16. M. Schulz and J. L. Keddie, *Soft Matter*, 2018, **14**, 6181-6197.

17. M. P. Howard, A. Nikoubashman and A. Z. Panagiotopoulos, *Langmuir*, 2017, **33**, 11390-11398.
18. P. K.-H. Ho, L.-L. Chua, M. Dipankar, X. Y. Gao, D. C. Qi, A. T.-S. Wee, J.-F. Chang and R. H. Friend, *Adv. Mater.*, 2007, **19**, 215-221.
19. R. Joseph Kline, M. D. McGehee and M. F. Toney, *Nat. Mater.*, 2006, **5**, 222-228.
20. Y. Zhong, J. Ma, K. Hashimoto and K. Tajima, *Adv. Mater.*, 2013, **25**, 1071-1075.
21. Y. Zhong, A. Tada, S. Izawa, K. Hashimoto and K. Tajima, *Adv. Energy Mater.*, 2014, **4**, 1301332.
22. K. Tajima, *Polym. J.*, 2019, **51**, 1117-1126.
23. N. J. Jeon, J. H. Noh, W. S. Yang, Y. C. Kim, S. Ryu, J. Seo and S. I. Seok, *Nature*, 2015, **517**, 476-480.
24. M. A. Mubarok, H. Aqoma, F. T. A. Wibowo, W. Lee, H. M. Kim, D. Y. Ryu, J.-W. Jeon and S.-Y. Jang, *Adv. Energy Mater.*, 2020, **10**, 1902933.
25. L. Bu, Z. Liu, M. Zhang, W. Li, A. Zhu, F. Cai, Z. Zhao and Y. Zhou, *ACS Appl. Mater. Interfaces*, 2015, **7**, 17776-17781.
26. Q. Wei, S. Miyanishi, K. Tajima and K. Hashimoto, *ACS Appl. Mater. Interfaces*, 2009, **1**, 2660-2666.
27. A. Tada, Y. Geng, Q. Wei, K. Hashimoto and K. Tajima, *Nat. Mater.*, 2011, **10**, 450-455.
28. S. J. Rinehart, G. Yuan and M. D. Dadmun, *Macromolecules*, 2018, **51**, 7836-7844.
29. B. Xue, B. Vaughan, C.-H. Poh, K. B. Burke, L. Thomsen, A. Stapleton, X. Zhou, G. W. Bryant, W. Belcher and P. C. Dastoor, *J. Phys. Chem. C*, 2010, **114**, 15797-15805.
30. R. Singhal, A. Chaubey, T. Srikhirin, S. Aphiwantrakul, S. S. Pandey and B. D. Malhotra, *Curr. Appl. Phys.*, 2003, **3**, 275-279.
31. K. H. Wang, W. P. Hsu, L. H. Chen, W. D. Lin and Y. L. Lee, *Colloids Surf. B*, 2017, **155**, 104-110.
32. L. J. Richter, D. M. DeLongchamp and A. Amassian, *Chem. Rev.*, 2017, **117**, 6332-6366.
33. K. W. Chou, B. Yan, R. Li, E. Q. Li, K. Zhao, D. H. Anjum, S. Alvarez, R. Gassaway, A. Biocca, S. T. Thoroddsen, A. Hexemer and A. Amassian, *Adv. Mater.*, 2013, **25**, 1923-1929.
34. K. Wei Chou, H. Ullah Khan, M. R. Niazi, B. Yan, R. Li, M. M. Payne, J. E. Anthony, D.-M. Smilgies and A. Amassian, *J. Mater. Chem. C*, 2014, **2**, 5681-5689.
35. T. Boublik, V. Fried and E. Hala, *The Vapor Pressures of Pure Substances, Second Revised Edition*, Amsterdam: Elsevier, 1984.
36. T. E. Daubert, Danne. R.P. , *Physical and Thermodynamic Properties of Pure Chemicals Data Compilation*, Washington, D.C.:Taylor and Francis, 1989.
37. Y. Jin, Z. Li, L. Qin, X. Liu, L. Mao, Y. Wang, F. Qin, Y. Liu, Y. Zhou and F. Zhang, *Adv. Mater. Interfaces*, 2017, **4**, 1700704.
38. K.-H. Yim, Z. Zheng, Z. Liang, R. H. Friend, W. T. S. Huck and J.-S. Kim, *Adv. Funct. Mater.*, 2008, **18**, 1012-1019.
39. Y. Zhong, M. Causa', G. J. Moore, P. Krauspe, B. Xiao, F. Günther, J. Kublitski, R. Shivhare, J. Benduhn, E. BarOr, S. Mukherjee, K. M. Yallum, J. Réhault, S. C. B. Mannsfeld, D. Neher, L. J. Richter, D. M. DeLongchamp, F. Ortmann, K. Vandewal, E. Zhou and N. Banerji, *Nat. Commun.*, 2020, **11**, 833.
40. R. Grzibovskis and A. Vembris, *J. Mater. Sci.*, 2018, **53**, 7506-7515.
41. Z.-L. Guan, J. B. Kim, Y.-L. Loo and A. Kahn, *J. Appl. Phys.*, 2011, **110**, 043719.
42. J. Xiao, J. Shi, H. Liu, Y. Xu, S. Lv, Y. Luo, D. Li, Q. Meng and Y. Li, *Adv. Energy Mater.*, 2015, **5**, 1401943.
43. G. Heimel, I. Salzmann, S. Duhm, J. P. Rabe and N. Koch, *Adv. Funct. Mater.*, 2009, **19**, 3874-3879.

44. J.-H. Kim, J.-A. Hong, D.-G. Kwon, J. Seo and Y. Park, *Appl. Phys. Lett.*, 2014, **104**, 163303.
45. K. Kanai, T. Miyazaki, T. Wakita, K. Akaike, T. Yokoya, Y. Ouchi and K. Seki, *Adv. Funct. Mater.*, 2010, **20**, 2046-2052.
46. N. Shioya, T. Shimoaka, K. Eda and T. Hasegawa, *Macromolecules*, 2017, **50**, 5090-5097.
47. R. Ghosh, C. M. Pochas and F. C. Spano, *J. Phys. Chem. C*, 2016, **120**, 11394-11406.
48. S. Sweetnam, K. R. Graham, G. O. Ngongang Ndjawa, T. Heumüller, J. A. Bartelt, T. M. Burke, W. Li, W. You, A. Amassian and M. D. McGehee, *J. Am. Chem. Soc.*, 2014, **136**, 14078-14088.
49. F. C. Jamieson, E. B. Domingo, T. McCarthy-Ward, M. Heeney, N. Stingelin and J. R. Durrant, *Chem. Sci.*, 2012, **3**, 485-492.
50. G. O. N. Ndjawa, K. R. Graham, S. Mollinger, D. M. Wu, D. Hanifi, R. Prasanna, B. D. Rose, S. Dey, L. Yu, J.-L. Brédas, M. D. McGehee, A. Salleo and A. Amassian, *Adv. Energy Mater.*, 2017, **7**, 1601995.
51. I. Ramirez, M. Causa', Y. Zhong, N. Banerji and M. Riede, *Adv. Energy Mater.*, 2018, **8**, 1703551.
52. K. R. Graham, P. Erwin, D. Nordlund, K. Vandewal, R. Li, G. O. Ngongang Ndjawa, E. T. Hoke, A. Salleo, M. E. Thompson, M. D. McGehee and A. Amassian, *Adv. Mater.*, 2013, **25**, 6076-6082.
53. C. Kästner, K. Vandewal, D. A. M. Egbe and H. Hoppe, *Adv. Sci.*, 2017, **4**, 1600331.
54. Y. Dong, V. C. Nikolis, F. Talnack, Y.-C. Chin, J. Benduhn, G. Londi, J. Kublitski, X. Zheng, S. C. B. Mannsfeld, D. Spoltore, L. Muccioli, J. Li, X. Blase, D. Beljonne, J.-S. Kim, A. A. Bakulin, G. D'Avino, J. R. Durrant and K. Vandewal, *Nat. Commun.*, 2020, **11**, 4617.
55. K. Nakano and K. Tajima, *Adv. Mater.*, 2017, **29**, 1603269.
56. K. Nakano, Y. Kaji and K. Tajima, *ACS Appl. Mater. Interfaces*, 2021, **13**, 28574-28582.
57. K. Nakano, T. Shibamori and K. Tajima, *ACS Omega*, 2018, **3**, 1522-1528.
58. W. C. Tsoi, D. T. James, J. S. Kim, P. G. Nicholson, C. E. Murphy, D. D. C. Bradley, J. Nelson and J.-S. Kim, *J. Am. Chem. Soc.*, 2011, **133**, 9834-9843.
59. S.-H. Lee, D.-H. Kim, J.-H. Kim, G.-S. Lee and J.-G. Park, *J. Phys. Chem. C*, 2009, **113**, 21915-21920.
60. G. Li, V. Shrotriya, J. Huang, Y. Yao, T. Moriarty, K. Emery and Y. Yang, *Nat. Mater.*, 2005, **4**, 864-868.
61. F. Laquai, D. Andrienko, R. Mauer and P. W. M. Blom, *Macromol. Rapid Commun.*, 2015, **36**, 1001-1025.
62. D. Chen, A. Nakahara, D. Wei, D. Nordlund and T. P. Russell, *Nano Lett.*, 2011, **11**, 561-567.
63. M. T. Dang, L. Hirsch and G. Wantz, *Adv. Mater.*, 2011, **23**, 3597-3602.
64. E. Lim, A. M. Glaudell, R. Miller and M. L. Chabinyc, *Adv. Electron. Mater.*, 2019, **5**, 1800915.
65. F. E. Osterloh, M. A. Holmes, L. Chang, A. J. Moulé and J. Zhao, *J. Phys. Chem. C*, 2013, **117**, 26905-26913.
66. H. Sirringhaus, P. J. Brown, R. H. Friend, M. M. Nielsen, K. Bechgaard, B. M. W. Langeveld-Voss, A. J. H. Spiering, R. A. J. Janssen, E. W. Meijer, P. Herwig and D. M. de Leeuw, *Nature*, 1999, **401**, 685-688.
67. N. D. Treat, M. A. Brady, G. Smith, M. F. Toney, E. J. Kramer, C. J. Hawker and M. L. Chabinyc, *Adv. Energy Mater.*, 2011, **1**, 82-89.
68. D. A. Chen, A. Nakahara, D. G. Wei, D. Nordlund and T. P. Russell, *Nano Lett.*, 2011, **11**, 561-567.

69. K. W. Chou, B. Y. Yan, R. P. Li, E. Q. Li, K. Zhao, D. H. Anjum, S. Alvarez, R. Gassaway, A. Biocca, S. T. Thoroddsen, A. Hexemer and A. Amassian, *Adv. Mater.*, 2013, **25**, 1923-1929.
70. V. S. Gevaerts, L. J. A. Koster, M. M. Wienk and R. A. J. Janssen, *ACS Appl. Mater. Interfaces*, 2011, **3**, 3252-3255.
71. Y. Cui, Y. Xu, H. Yao, P. Bi, L. Hong, J. Zhang, Y. Zu, T. Zhang, J. Qin, J. Ren, Z. Chen, C. He, X. Hao, Z. Wei and J. Hou, *Adv. Mater.*, 2021, **n/a**, 2102420.
72. H. Chen, T. Zhao, L. Li, P. Tan, H. Lai, Y. Zhu, X. Lai, L. Han, N. Zheng, L. Guo and F. He, *Adv. Mater.*, 2021, **33**, 2102778.
73. Y. Wang, Q. Zhu, H. B. Naveed, H. Zhao, K. Zhou and W. Ma, *Adv. Energy Mater.*, 2020, **10**, 1903609.
74. Y. Zhong, S. Izawa, K. Hashimoto, K. Tajima, T. Koganezawa and H. Yoshida, *J. Phys. Chem. C*, 2015, **119**, 23-28.
75. M. Lenes, G.-J. A. H. Wetzelaer, F. B. Kooistra, S. C. Veenstra, J. C. Hummelen and P. W. M. Blom, *Adv. Mater.*, 2008, **20**, 2116-2119.
76. D. Baran, R. S. Ashraf, D. A. Hanifi, M. Abdelsamie, N. Gasparini, J. A. Röhr, S. Holliday, A. Wadsworth, S. Lockett, M. Neophytou, C. J. M. Emmott, J. Nelson, C. J. Brabec, A. Amassian, A. Salleo, T. Kirchartz, J. R. Durrant and I. McCulloch, *Nat. Mater.*, 2017, **16**, 363-369.
77. W. C. Tsoi, S. J. Spencer, L. Yang, A. M. Ballantyne, P. G. Nicholson, A. Turnbull, A. G. Shard, C. E. Murphy, D. D. C. Bradley, J. Nelson and J.-S. Kim, *Macromolecules*, 2011, **44**, 2944-2952.
78. A. C. Jakowetz, M. L. Böhm, A. Sadhanala, S. Huettner, A. Rao and R. H. Friend, *Nat. Mater.*, 2017, **16**, 551-557.
79. J. Benduhn, K. Tvingstedt, F. Piersimoni, S. Ullbrich, Y. Fan, M. Tropiano, K. A. McGarry, O. Zeika, M. K. Riede, C. J. Douglas, S. Barlow, S. R. Marder, D. Neher, D. Spoltore and K. Vandewal, *Nat. Energy*, 2017, **2**, 17053.
80. A. R. Kirmani, G. Walters, T. Kim, E. H. Sargent and A. Amassian, *ACS Appl. Energy Mater.*, 2020, **3**, 5385-5392.
81. J. M. Luther, M. Law, Q. Song, C. L. Perkins, M. C. Beard and A. J. Nozik, *ACS Nano*, 2008, **2**, 271-280.
82. A. R. Kirmani, A. D. Sheikh, M. R. Niazi, M. A. Haque, M. Liu, F. P. G. de Arquer, J. Xu, B. Sun, O. Voznyy, N. Gasparini, D. Baran, T. Wu, E. H. Sargent and A. Amassian, *Adv. Mater.*, 2018, **30**, 1801661.
83. H. Aqoma, M. A. Mubarok, W. Lee, W. T. Hadmojo, C. Park, T. K. Ahn, D. Y. Ryu and S.-Y. Jang, *Adv. Energy Mater.*, 2018, **8**, 1800572.
84. Y. Zhang, Y. Kan, K. Gao, M. Gu, Y. Shi, X. Zhang, Y. Xue, X. Zhang, Z. Liu, Y. Zhang, J. Yuan, W. Ma and A. K. Y. Jen, *ACS Energy Lett.*, 2020, **5**, 2335-2342.
85. Y. Xue, F. Yang, J. Yuan, Y. Zhang, M. Gu, Y. Xu, X. Ling, Y. Wang, F. Li, T. Zhai, J. Li, C. Cui, Y. Chen and W. Ma, *ACS Energy Lett.*, 2019, **4**, 2850-2858.
86. H. I. Kim, J. Lee, M.-J. Choi, S. U. Ryu, K. Choi, S. Lee, S. Hoogland, F. P. G. de Arquer, E. H. Sargent and T. Park, *Adv. Energy Mater.*, 2020, **10**, 2002084.